The 2009 IEEE/RSJ International Conference on
Intelligent Robots and Systems
October 11-15, 2009 St. Louis, USA

Terrain Surface Classification for Autonomous Ground Vehicles Using a 2D Laser Stripe-Based Structured Light Sensor

Liang Lu, Camilo Ordonez, Emmanuel G. Collins, Jr. and Edmond M. DuPont

Abstract— **To increase autonomous ground vehicle (AGV) safety and efficiency on outdoor terrains the vehicle's control system should have settings for individual terrain surfaces. A first step in such a terrain-dependent control system is classification of the surface upon which the AGV is traversing. This paper considers vision-based terrain surface classification for the path directly in front of the vehicle (< 1 m). Most vision-based terrain classification has focused on terrain traversability and not on terrain surface classification. The few approaches to classifying traversable terrain surfaces, with the exception of the use of infrared cameras to classify mud, have relied on stand-alone cameras that are designed for daytime use and are not expected to perform well in the dark. In contrast, this research uses a laser stripe-based structured light sensor, which uses a laser in conjunction with a camera, and hence can work at night. Also, unlike most previous results, the classification here does not rely on color since color changes with illumination and weather, and certain terrains have multiple colors (e.g., sand may be red or white). Instead, it relies only on spatial relationships, specifically spatial frequency response and texture, which captures spatial relationships between different gray levels. Terrain surface classification using each of these features separately is conducted by using a probabilistic neural network. Experimental results based on classifying four outdoor terrains demonstrate the effectiveness of the proposed methods.**

I. INTRODUCTION

Autonomous ground vehicles (AGVs) are increasingly being used and considered for outdoor tasks in unstructured environments. These tasks include agricultural applications, fire fighting, search and rescue missions, as well as military missions. It follows that AGVs will be required to traverse a variety of terrain surfaces. To enable safe and efficient traversal, a vehicle's control system may be tuned to a given surface. An example of such a control system is the Terrain Response system available on many Land Rovers [1]. This system has modes for everyday driving, grass/gravel/snow, mud and ruts, sand, and rock crawls. Each mode has predefined settings that change vehicle parameters such as anti-lock braking, throttle response, and differential locking. Terrain-dependent AGV guidance can also involve limits on turn radius and speed, tire pressure adjustments, rut following, etc. In manned systems, these adjustments are made once the driver recognizes a change in terrain. However, for AGVs automated terrain classification is essential.

Terrain surface classification methods for mobile robots have two main categories, those based on proprioceptive (i.e., vibration and slip) sensors [2], [3], [4], [5], [6], [7], [8], [9] and those based on vision sensors [10], [11], [12], corresponding respectively to "feeling" and "seeing." Unlike proprioceptive sensors, which are often associated with an inertial measurement unit, vision sensor measurements are essentially independent of the speed and load of the vehicle. However, vision sensors can lead to false classifications when the ground has a superficial covering (e.g., leaves, dry grass, or a small amount of water) or when the environment has reduced visibility due to smoke, fog or other precipitation. They may also fail to discern between surfaces that have a similar appearance, but are very distinct from a control perspective, such as dry and wet sand or dirt and mud. Hence, what is needed is a synergy of the two basic approaches to terrain classification. Initial results for this synergy are given in [11].

This paper focuses exclusively on surface classification for traversable terrains using vision sensors. Very few vision-based approaches to this problem have appeared in the literature to date. The research of [10] used a long range camera and classified large terrain patches using features such us average red, average color, 3D color histogram, and texture metrics. Parallel research in [11] used cameras at short range to detect terrains in close proximity to planetary rovers on Mars-like environments.[1] In addition, short-wave, mid-wave and long-wave infrared cameras, which do work at night, were used in [12] to classify mud. Additional research presented in [13], proposed an image-retrieval approach that utilizes wavelet signatures to estimate the size of fine particles in mineral ore. This research has potential to be used in the domain of surface classification. The terrains classified in the present research are similar to those classified in [10] and [11]. However, this research uses a *laser line striper* [14], which is used here as shorthand for a *laser stripe-based structured light sensor* [15].

A laser line striper is a high resolution, low proximity, hybrid sensor, consisting of a single infrared camera and a single laser. An advantage that this sensor has over a stand-alone camera is that it is an active sensor, due to the laser, and is hence capable of classifying terrains at night. The laser line striper captures the intersection line between the laser plane and the terrain. Compared with a standard laser scanner with a 180° or 360° field of view, the laser line striper has only a 30° field of view. However, it is sufficient for this research. The object of this research is to detect a small patch of terrain at close range (< 1 m), directly in front of the vehicle. The laser line striper has higher resolution, 0.05° angular resolution and 4 mm range resolution. In contrast, the angular resolution and range resolution of a SICK laser LMS 200 are 0.25° and 10 mm. The higher resolution of the laser line striper is expected to lead to higher classification

[1]The results were based on actual camera data form Mars

accuracies, although this remains to be shown.

Since color may change under different illumination and weather conditions and also certain terrains may have more than one color, e.g., grass may be green or yellow and sand may be red or white, the methodology used for classification, unlike that in [10] and [11], does not rely on color; instead it relies only on spatial relationships, specifically spatial frequency response and texture, which captures spatial relationships between different gray levels. Terrain classification using each of these features separately is conducted by using a probabilistic neural network [16], similar to its use in [6], [7], [8], [9].

Most prior classification research based on the use of optical or laser-based sensors [17], [18], [19], [20], [21], [22] has focused on classifying terrain to determine traversability or non-traversability. Traversability classification in [17] uses cameras and is approached by characterizing the terrain in terms of roughness, slope, discontinuities, and hardness. The research of [18] used a multispectral sensor to distinguish between pliable vegetation and true mobility obstacles. The research of [19] used a 2D laser scanner to discriminate between obstacles and traversable terrain. Additional research classifies terrains into broad categories. For example, the research of [20] and [21] used three far range sensing ladars ($\geq$ 10 m), Z+F LARA 21400, the LADAR used on the GDRS XUVs and Acuity AccuRange 4000, to distinguish ground and vegetation. The research of [22], which also used three far range sensing ladars, SICK laser LMS 291, Z+F LARA 21400 and Riegl LMS-Z210, performed 3D data segmentation for classifying terrain into three categories: "scatter" (porous volumes such as grass or tree canopy), "linear" (thin objects) and "surface" (solid objects).

This paper is organized as follows. Section II presents the proposed approach. Section III describes the experimental setup and presents the results of the experiments conducted on four different outdoor terrains. Section IV presents concluding remarks and directions for future research.

II. PROPOSED APPROACH

The proposed terrain classification method is composed of three stages, data collection, feature extraction and classification, as described below.

A. Data Collection

Data from four terrains, asphalt, grass, gravel and sand, was collected. While the robot traversed different terrains, the laser line striper mounted on the robot collected the terrain images. Figure 1 shows how a laser line striper works. The basic principle of operation is triangulation. The laser line striper consists of an infrared laser and an infrared camera. The light of a laser is fanned out in about 60° to form a plane of light. If an object or ground intersects the laser plane, the reflected light is observed by a camera placed at a distance from the laser. The camera generates images containing the intersection line of a laser plane and the terrain being traversed by the robot. The size of each terrain patch captured by the camera is about 45 cm $\times$ 35 cm. The images

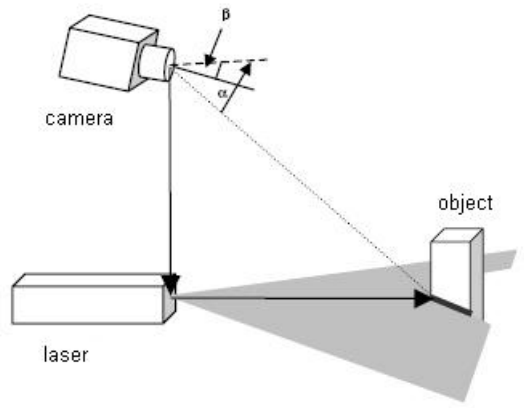

Fig. 1. Geometric configuration of a laser line striper.

are grayscale images in resolution of 640 $\times$ 480, collected at a rate of 15 frames/second. After the image was collected, the terrain classification algorithm proceeded with the feature extraction stage.

B. Feature Extraction

Two different features, spatial frequency response and texture, were used separately to characterize the terrain. In this discussion four common terrains are explicitly considered: asphalt, grass, gravel and sand. However, the classification methodology is applicable to a greater number of terrains.

1) Spatial frequency response: Unlike texture, the spatial frequency response does not take advantage of the intensity data provided by the camera in the laser line striper. However, an accurate frequency response results from the high spatial resolution provided by the laser line striper. This feature also provides a direct link between vision-based classification and vibration-based classification [6], [7]. In fact, as discussed in [7], the terrain signature in the frequency response of the vehicle vibrations is a direct result of the spatial frequency response terrain signature that is shown by the results of this paper.

To compute the spatial frequency response feature, the laser line points are first extracted from the image and are then transformed from the image coordinates to the laser plane coordinates (x, y) following a homogeneous transformation that is obtained as a result of calibrating the laser line striper [14]. This new set of points in laser plane coordinates is used to represent the terrain profile. Figure 2 shows the raw images of four different terrains captured by the line striper and the resulting terrain profiles.

Before finding the frequency contents of the terrain profiles, it is important to remove information that is not inherent to the terrain type like the zero frequency (DC) component and the average slope of the profile. The DC component represents the average height of the profile and is removed by subtracting the average y-value from the y component of each point in the profile. The slope characterizes the average incline/decline of the terrain surface to be traversed. The

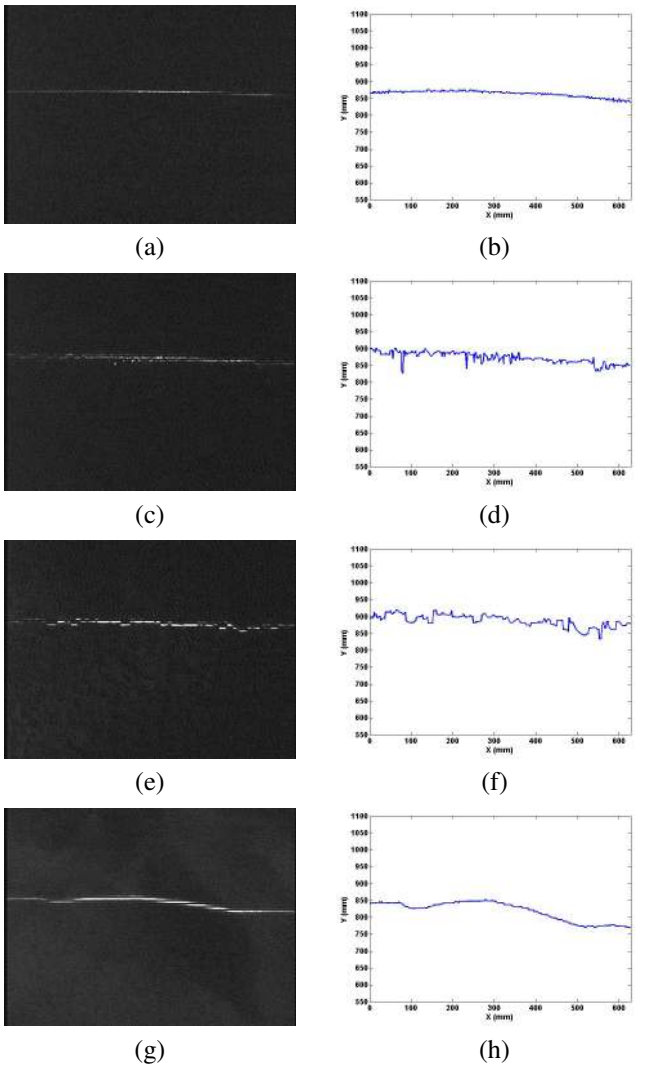

Fig. 2. Raw laser line images (left column) and extracted terrain profiles (right column) for asphalt (a),(b); grass (c),(d); gravel (e),(f); and sand (g),(h).

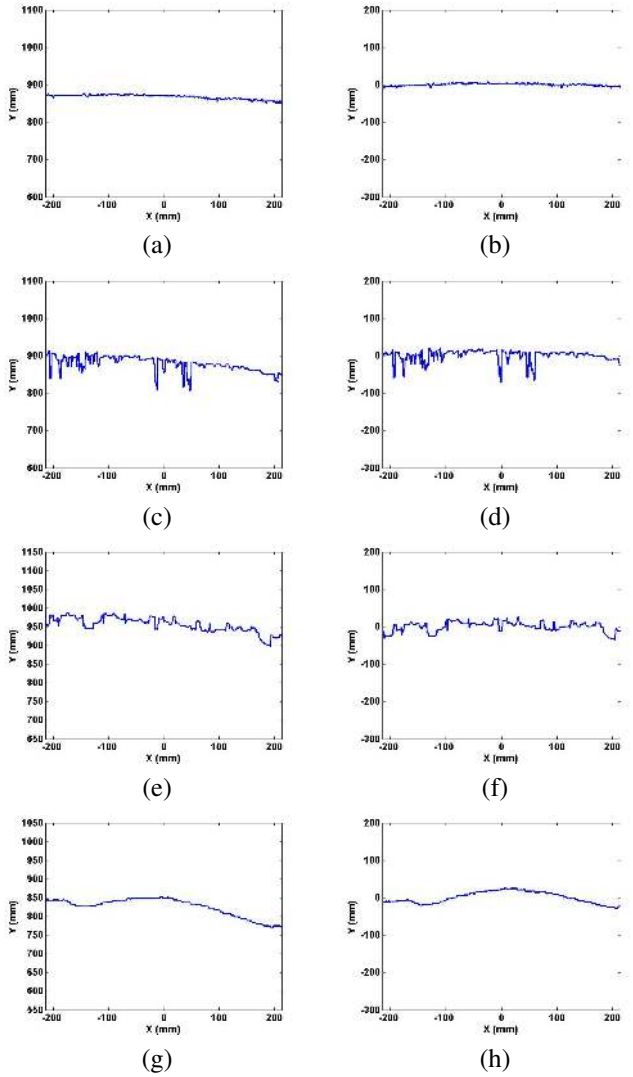

Fig. 3. Terrain profiles of asphalt before (left column) and after (right column) slope and DC component elimination for asphalt (a),(b); grass (c),(d); gravel (e),(f); and sand (g),(h).

slope discussed here is the relative slope with respect to the robot. The slope information is removed by fitting a line in the least squares sense to the profile, and subtracting the corresponding predicted value obtained using the approximating line from the y component of each point on the profile. Figure 3 presents the terrain profiles before and after the elimination of the DC component and slope.

The new terrain profile y-values obtained after the elimination of the DC component and slope form a discrete sequence $y[n]$ with length equal to the number of laser points. To find the frequency components of $y[n]$, the spatial Fourier transform of $y[n]$ is obtained by using the Fast Fourier Transform (FFT). The magnitude of the frequency response is chosen as the frequency based feature vector.

Figure 4 shows the frequency domain representation of the four different terrain profiles being considered. Notice that asphalt has the flattest response because asphalt has the flattest surface among these four terrains. Grass and gravel have similar frequency responses, especially at low frequency. Fortunately, they are different at high frequency. Gravel converges to zero more quickly than grass. Sand possesses substantial low frequency content due to the low frequency undulations that naturally occur in sand.

2) Texture: Although no formal definition of texture exists, intuitively this descriptor provides measures of properties such as smoothness, coarseness, and regularity [23]. To characterize texture it is necessary to characterize the gray level primitive properties as well as the spatial relationships between them [24].

In this paper, a statistical approach based on the Gray-Level Co-occurrence Matrix (GLCM) [23] is chosen to describe the texture of the laser line striper images. To quantify the texture content of the laser line striper images, a set of descriptors from the GLCM are obtained.

The GLCM can be specified in a matrix of relative frequencies $p(i, j)$ in which two adjacent pixels occur on the image, one with gray level i and the other with gray

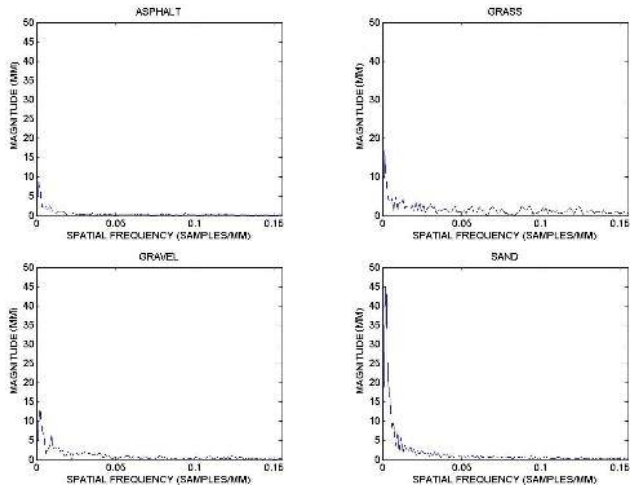

Fig. 4. Frequency domain representation of the terrain profiles.

level j [24]. The following textural features are chosen to quantify the texture content of the images:

1) *Contrast*: Measures the local variations in the GLCM, given by

$$\sum_{i,j} |i-j|^2 p(i,j). \tag{1}$$

2) *Correlation*: Measures how correlated a pixel is to its neighbor over the whole image, which is mathematically described by

$$\sum_{i,j} \frac{(i-\mu_i)(j-\mu_j)p(i,j)}{\sigma_i \sigma_j}, \tag{2}$$

where

$$\mu_i = \sum_i i \sum_j p(i,j), \quad \mu_j = \sum_j j \sum_i p(i,j), \tag{3}$$

$$\sigma_i = \sum_i (i-\mu_i)^2 \sum_j p(i,j), \tag{4}$$

$$\sigma_j = \sum_j (j-\mu_j)^2 \sum_i p(i,j). \tag{5}$$

3) *Energy*: Provides a measure of uniformity, given by

$$\sum_{i,j} p^2(i,j) \tag{6}$$

4) *Homogeneity*: Measures the closeness of the distribution of elements in the GLCM to the GLCM diagonal, mathematically described by

$$\sum_{i,j} \frac{p(i,j)}{1+|i-j|} \tag{7}$$

The texture feature vector $\mathbf{x}_t$ is then chosen as the 4 dimensional vector,

$$\mathbf{x}_t = [Contrast\ Correlation\ Energy\ Homogeneity], \tag{8}$$

such that each component represents a texture metric. Figure 5 shows texture descriptors for a representative sample of each of the four terrains. (Note that for ease of visualization, the values of contrast are 100 times larger than the actual values.) Three descriptors, correlation, energy and homogeneity are dominant in magnitude. They have distinct patterns for most terrains, but asphalt and gravel do have similar patterns. Fortunately, these two terrains have distinct contrast values.

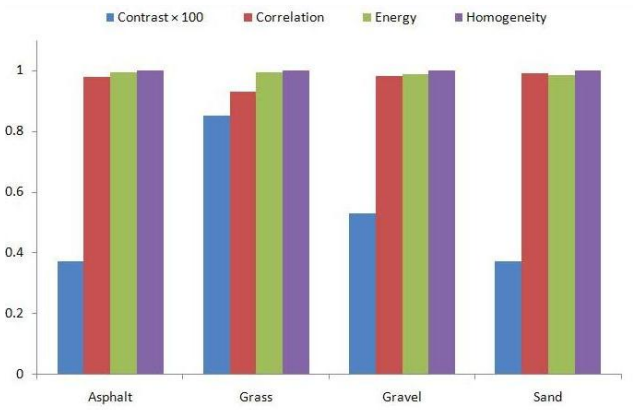

Fig. 5. Texture descriptors for representative samples of four terrains.

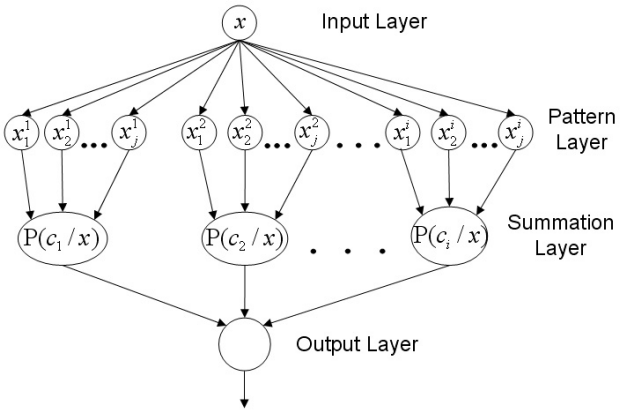

Fig. 6. Architectural structure of probabilistic neural network.

C. Classification

A probabilistic neural network (PNN) was selected to classify the feature vector $\mathbf{x}$ as a particular terrain. It was chosen because of its simplicity, robustness to noise and fast training speed [16].

The PNN is based on Bayesian classifiers and uses a supervised training set to develop distribution functions. These functions are used to estimate the likelihood of an input feature vector being part of a learned category or class. The learned patterns can also be combined or weighted with the a priori probability of each category to determine the most likely class for a given input vector. If the relative frequency of the categories is unknown, then all categories can be assumed to be equally likely and the determination of category is solely based on the closeness of the input feature vector to the distribution function of a class [25].

Fig. 7. Experimental platform.

The network structure of the PNN is shown in Figure 6. The network has an input layer, a pattern layer, a summation layer, and an output layer [26]. The input layer buffers the input feature vector $\mathbf{x}$ to the neurons in the pattern layer. Then, the neuron $\mathbf{x}_j^i$ computes its output using

$$\phi_{ij}(\mathbf{x}) = \frac{1}{(2\pi)^{\frac{N}{2}}\sigma^N} \exp\left[-\frac{(\mathbf{x}-\mathbf{x}_j^i)^T(\mathbf{x}-\mathbf{x}_j^i)}{2\sigma^2}\right], \quad (9)$$

where i is the class, in this research is the terrain type, j is the training sample in class i, σ is a smoothing factor, and N is the dimension of the pattern vector $\mathbf{x}$. The summation layer uses a Parzen window [27], with a Gaussian distribution as the window function, to compute the probability $P(C_i|\mathbf{x})$ of a given input $\mathbf{x}$ belonging to a class C_i. In particular,

$$P(C_i|\mathbf{x}) = \frac{1}{(2\pi)^{\frac{N}{2}}\sigma^N} \sum_{j=1}^{n_i} \exp\left[-\frac{(\mathbf{x}-\mathbf{x}_j^i)^T(\mathbf{x}-\mathbf{x}_j^i)}{2\sigma^2}\right], \quad (10)$$

where n_i denotes the total number of samples in class C_i. The output layer uses the calculation of the probability distribution function from the summation layer, and applies the decision rule of (11) to select the class with the highest probability.

The vector $\mathbf{x}$ is said to belong to a particular class C_i if

$$P(C_i|\mathbf{x}) > P(C_j|\mathbf{x}),\ \forall j = 1, 2 \cdot \cdot, n,\ j \neq i. \quad (11)$$

The selection of the smoothing factor σ has great influence on the performance of the PNN. For nonlinear decision boundaries, the smoothing factor needs to be as small as possible [6]. We use the method of cross-validation to select a suitable smoothing factor. The original data is divided into three sets: training data, testing data and cross-validation data. The cross-validation data is used to tune the smoothing factor until the PNN produces the desired performance.

III. EXPERIMENTS AND RESULTS

A. Experimental Setup

The robotic platform used in the experiments is the ATRV Jr, shown in Figure 7. This vehicle is a skid steered robot that weighs 50 kg and has a maximum translational speed of 1400 mm/sec.

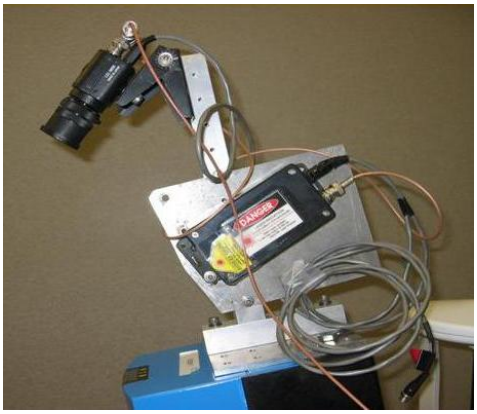

Fig. 8. Laser line striper.

Mounted on the ATRV Jr. is a laser line striper sensor provided by the Carnegie Mellon University Robotics Institute. This particular sensor will hence be subsequently referred to as the *CMU Line Striper*. The height of the laser is 37 cm and it pointed 25° downward with respect to the horizontal plane. The height of the camera is 53 cm and it pointed 48° downward with respect to the horizontal plane. Figure 8 provides a closeup view of the CMU Line Striper. This sensor has a unique set of features that make it useful for this terrain classification research.

1) *Illumination Robustness*: This sensor is designed to work under different illumination conditions (e.g., any time of day or night). To make this possible, the system suppresses background from the sun by employing an IR (GaAs 900 nm) pulsed laser, a fast camera shutter (1/100,000 second) and a narrow filter (25 nm) placed between the camera lens, and the CCD sensor.
2) *High Angular Resolution*: The sensor provides high angular resolution. The current set up uses a 30° field of view camera, which achieves an angular resolution of 0.05°.
3) *Real-Time Operation*. This feature is obviously important for real-time terrain classification, an ultimate aim of this research.
4) *Provides Range and Intensity Information*: Due to the usage of both a laser and a camera, both range and intensity information are provided by the system.
5) *Small Size*: This sensor is suitable for use with relatively small robots.
6) *Low Cost*: If mass produced, this sensor is expected to cost on the order of $100.
7) *Eye Safe*: This is a critical feature for the numerous applications in which a robot will operate in the presence of humans.

B. Experimental Procedure

A set of outdoor experiments were conducted on the four common terrains shown in Figure 9: asphalt, grass, gravel and sand. For each type of terrain the robot was commanded to travel for 10 sec at speeds in the range of 100 mm/sec to 1000 mm/sec. During each run, the CMU

Fig. 9. Outdoor terrains.

Fig. 10. Small terrain patches for indoor experiments.

Line Striper images were collected at a rate of 15 Hz. These images constitute the perception data employed to classify the different terrains. It is important to clarify that although it is expected that vision based techniques have little dependence on speed (especially at low speeds), here an attempt is made to minimize any speed dependence by combining the data collected at different speeds into a vector set used for classification. However, further studies should be conducted to properly quantify speed dependencies of vision based approaches over large speed ranges.

A smaller set of indoor experiments were also conducted to prove that the laser line striper can also work at night (i.e., in the dark). Figure 10 shows the three types of terrain that were brought indoors to enable testing in a controlled light environment. In the process of the experiments, the light luminance was changed to imitate evening and night and the luminance was measured using the Extech EasyView digital light meter EA30. The light was due to the fluorescent ceiling lights in the lab. The classification experiments were run under four different light conditions: 1) *All lights on*. (The luminance was 653 lux.) 2) *Half of the lights on*. (The luminance was 338 lux.) 3) *The other half of the lights on*. (The luminance was 293 lux.) 4) *All lights off*. (The luminance was 0.24 lux.) The data collected under light condition 1 was used as training data. The data collected under other light conditions was used as testing data. As shown in Subsection III-C, the classification accuracies resulting from the indoor experiments were very similar to those for the outdoor experiments and did not vary with illumination.

In previous experiments, the robot only traversed on white sand. Hence, another small set of experiments was conducted on red sand in order to check the color robustness. The robot ran one trial at 200 mm/sec, 400 mm/sec and 600 mm/sec. Figure 11 shows the comparison of white sand and red sand.

Fig. 11. The comparison of white sand and red sand.

TABLE I

SPATIAL FREQUENCY RESPONSE CLASSIFICATION RESULTS

		Training Data			
		Asphalt	Grass	Gravel	Sand
Testing Data	Asphalt	98.8%	0.0%	0.0%	1.2%
	Grass	0.0%	86.0%	12.8%	1.2%
	Gravel	0.0%	4.8%	93.4%	1.8%
	Sand	6.0%	0.6%	1.2%	92.2%

C. Classification Results

This section presents classification results obtained using the different features described in Subsection II-B.

1) Spatial frequency response: Table I shows classification results using the frequency response method. The results show that spatial frequency response is an efficient terrain signature. The algorithm classified the four terrains with greater than 86.0% accuracy. Grass and gravel are the two terrains that were most often confused. This was not surprising since in Figure 4 grass and gravel have similar frequency responses, especially at low frequency. Sand has the largest variability, i.e., it may be misclassified as all of the remaining terrains and all of the remaining terrains may be misclassified as sand. This is because sand terrains are sometimes as flat as asphalt and sometimes display coarser patterns that may be confused with gravel or grass.

2) Texture: Table II shows classification results using the textural features for classification. The result shows that texture is also an efficient terrain signature. The algorithm classified the four terrains with greater than 89.0% accuracy. Grass was always classified correctly. As for misclassification, 10.6% of gravel was classified as asphalt and 5.0% of sand was classified as gravel. This corresponds with Figure 5, which shows asphalt, gravel and sand have relatively close values of texture descriptors, especially asphalt and gravel.

3) Results comparison: Figure 12 shows the results comparison between the method of spatial frequency response and texture. Both of these two methods resulted in satisfactory classification results. The accuracy for each type of terrain was above 85.0%. For asphalt and sand the two methods gave almost the same results. For grass texture provided 14.0% better classification accuracy than spatial frequency response, while for gravel spatial frequency response provided 4.4% better classification accuracy than texture.

TABLE II

TEXTURE CLASSIFICATION RESULTS

		Training Data			
		Asphalt	Grass	Gravel	Sand
Testing Data	Asphalt	99.2%	0.0%	0.8%	0.0%
	Grass	0.0%	100.0%	0.0%	0.0%
	Gravel	10.6%	0.0%	89.0%	0.4%
	Sand	1.4%	1.0%	5.0%	92.6%

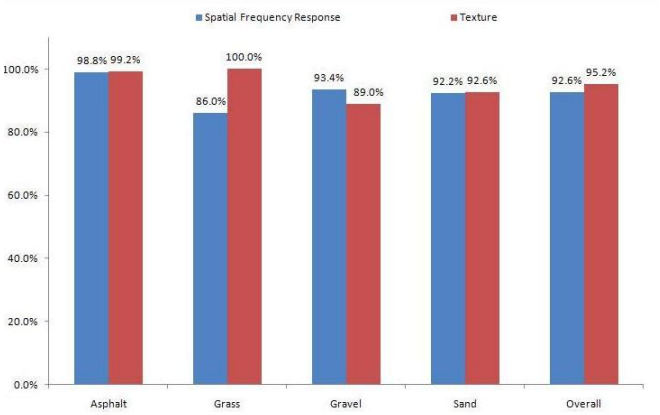

Fig. 12. Comparison of classification accuracies corresponding to classification based on spatial frequency response and texture.

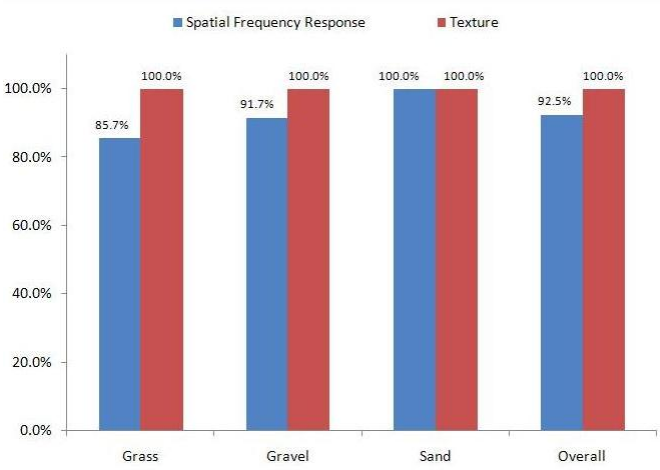

Fig. 13. Classification accuracies for indoor experiments under different illumination conditions.

TABLE III

RED SAND CLASSIFICATION RESULTS

Testing		Training Data			
		Asphalt	Grass	Gravel	Sand
Red Sand	Frequency	0.0%	0.0%	0.0%	100.0%
	Texture	7.9%	0.0%	4.8%	87.3%

Texture gave a slightly higher (2.6%) overall classification accuracy than spatial frequency response.

As discussed above in Subsections III-C.1 and III-C.2, the two sets of terrain signatures, spatial frequency response and texture, have advantages in distinguishing between some terrains but may find it more difficult to distinguish between another set of terrains. For example, grass and gravel have similar frequency responses but distinct textures. Hence, It is better to use texture than spatial frequency response to classify these two terrains. Asphalt and gravel have distinct frequency responses but similar textures. Hence, it is better to use spatial frequency response than texture to classify these two terrains.

4) Indoor experiments result: Figure 13 shows the result of the indoor experiments under different illumination conditions. Similar to the outdoor experiments, the accuracy for each type of terrain was above 85.0%, but the indoor experiments yielded better result than the outdoor experiments. The main reason is that the influences of some common features of outdoor terrain were eliminated, in particular, the nonhomogeneity of terrain and the terrain roughness. For example, outdoor gravel is often not pure gravel. It frequently contains elements of grass, sand and other objects. Hence, when gravel data is collected, it is corrupted with non-gravel information. In contrast, the terrains used for the indoor experiments were very homogenous and smoother than the outdoor terrains. Also, when the robot traverses indoors, it does not vibrate up and down due to "waves" in the terrain. Snapshooting while vibrating results in blurred images, which make it more difficult to perceive the terrain signatures. On the other hand, the smooth robot motion of the indoor experiments led to higher quality images and more pure terrain signatures. In contrast to the outdoor experiment, texture provided better classification accuracy than spatial frequency response not only for grass but also for gravel. This indicates that texture signatures are more corrupted from the nonidealities of the outdoor terrains.

5) Red sand experiments result: Table III shows classification results of the experiments conducted on red sand. The testing data used the information collected from red sand. The terrain classification algorithm was tested using the previously trained probabilistic neural network, which only included white sand information. Spatial frequency response classified red sand perfectly as sand. It has good color robustness. Texture classified red sand with a high accuracy of 87.3%.

IV. CONCLUSIONS

This paper presents a new method for vision-based terrain classification using close range sensing. Unlike previous research, this classification does not rely on color. It relies on spatial relations. To our knowledge, this research is the first to use spatial dependence features for vision-based terrain classification. Two features were developed, spatial frequency response and texture, which presents the spatial relationships between different gray levels. A laser stripe-based structured light sensor was used for the experiments and this was the first time this type of sensor was used for terrain classification. The range information proved to be useful in determining the spatial frequency content of the terrain profiles. The high resolution of the laser line striper allowed a very localized texture analysis of the terrain images. Outdoor experimental results on four different

terrains show the effectiveness of the proposed method. The overall classification result is above 90%. The results also show that each feature has advantages in classifying some terrains and disadvantages in classifying other terrains. In addition, the indoor, light-controlled and color experiments show that the spatial frequency response and texture features have luminance robustness and color robustness.

All the experiments were conducted on a low speed robot. The classification speed and sensing technology may limit the method's application to a high speed vehicle. In the future, some experiments need to be conducted to find the maximum speed boundary for this method. In addition, the proposed approach was tested in relatively homogeneous terrains. Therefore, more challenging experiments involving mixed terrains and surfaces with anisotropic features (e.g. concrete roadways with grooves in predefined directions) should be conducted to determine the range of applicability of the proposed approach.

Because each feature has advantages in classifying certain terrains, finding a good way to use both of these features together can overcome misclassification and yield better classification accuracy. A modified probabilistic neural network may need to be developed. Besides a synergy of the two features, a synergy of two basic terrain classification approaches, vision-based and vibration-based, is also important and valuable. Future work will involve taking advantage of the two basic approaches to terrain classification.

V. ACKNOWLEDGMENTS

The authors thank Christoph Mertz and Martial Hebert from the Carnegie Mellon University Robotics Institute for providing the laser line striper used in this research.

Prepared through collaborative participation in the Robotics Consortium sponsored by the U. S. Army Research Laboratory under the Collaborative Technology Alliance Program, Cooperative Agreement DAAD 19-01-2-0012. The U. S. Government is authorized to reproduce and distribute reprints for Government purposes notwithstanding any copyright notation thereon.

REFERENCES

[1] D. Vanderwerp. What does terrain response do? http://www.caranddriver.com/features/9026/what-does-terrain-response-do.html, February 2005.

[2] K. D. Iagnemma and S. Dubowsky. Terrain estimation for high-speed rough-terrain autonomous vehicle navigation. In *Proceedings of the SPIE Conference on Unmanned Ground Vehicle Technology IV*, volume 4715, July 2002.

[3] D. Sadhukhan and C. Moore. Online terrain estimation using internal sensors. In *Proceedings of the Florida Conference on Recent Advances in Robotics*, Boca Raton, FL, May 2003.

[4] D. Sadhukhan. Autonomous ground vehicle terrain classification using internal sensors. Master's thesis, Florida State University, Tallahassee, FL, March 2004.

[5] L. Ojeda, J. Borenstein, G. Witus, and R. Karlesen. Terrain characterization and classification with a mobile robot. *Journal of Field Robotics*, 23(2):103–122, January 2006.

[6] E. M. DuPont, R. G. Roberts, C. A. Moore, M. F. Selekwa, and E. G. Collins. Online terrain classification for mobile robots. In *Proceedings of IMECE 2005 ASME 2005 International Mechanical Engineering Congress and Exposition Conference*, Orlando, FL, November 2005.

[7] E. G. Collins Jr. and E. Coyle. Vibration-based terrain classification using surface profile input frequency responses. In *IEEE International Conference on Robotics and Automation*, pages 3276 – 3283, May 2008.

[8] E. M. Dupont, C. A. Moore, Jr. E. G. Collins, and E. Coyle. Frequency response method for terrain classification in autonomous ground vehicles. *Autonomous Robots*, 24(4):337–347, May 2008.

[9] E. M. DuPont, E. G. Collins, E. J. Coyle, and R. G. Roberts. *New Research on Mbile Robotics*, chapter Terrain classification using vibration sensors: theory and methods. Nova Science Publishers, to appear, 2008.

[10] A. Angelova, L. Matthies, D. Helmick, and P. Perona. Fast terrain classification using variable-length representation for autonomous navigation. In *IEEE Computer Society Conference on Computer Vision and Pattern Recognition*, pages 1–8, June 2007.

[11] I. Halatci, C. A. Brooks, and K. Iagnemma. Terrain classification and classifier fusion for planetary exploration rovers. In *IEEE Aerospace Conference*, pages 1–11, March 2007.

[12] A. Rankin and L. Matthies. Daytime mud detection for unmanned ground vehicle autonomous navigation. In *Proceedings of the 26th Army Science Conference*, December 2008.

[13] Ming Hong Pi and Hong Zhang. Measurement of fine particle size with wavelet signature. In *Image Processing, 2005. ICIP 2005. IEEE International Conference on*, volume 3, pages III–165–8, Sept. 2005.

[14] C. Mertz, J. Kozar, J. R. Miller, and C. Thorpe. Eye-safe laser line striper for outside use. In *IV 2002, IEEE Intelligent Vehicle Symposium, June, 2002*, December 2001.

[15] R. Siegwart and I. R. Nourbakhsh. *Introduction to Autonomous Mobile Robots*. The MIT Press, 2004.

[16] D. F. Specht. Probabilistic neural networks. *Neural Networks*, 3(1):109–118, 1990.

[17] A. Howard and H. Seraji. Vision-based terrain characterization and traversability assesment. *Journal of Robotic Systems*, 18(10):577–587, Sept. 2001.

[18] D. Bradley, S. Thayer, A. Stentz, and P. Rander. Vegetation detection for mobile robot navigation. Technical Report CMU-RI-TR-04-12, Robotics Institute, Carnegie Mellon University, Pittsburgh, PA, February 2004.

[19] J. C. Andersen, M. R. Blas, O. Ravn, N. A. Andersen, and M. Blanke. Traversable terrain classification for outdoor autonomous robots using single 2d laser scans. *Integr. Computer-Aided Engineering*, 13(3):223–232, 2006.

[20] M. Hebert, N. Vandapel, S. Keller, and R. R. Donamukkala. Evaluation and comparison of terrain classification techniques from ladar data for autonomous navigation. In *23rd Army Science Conference*, December 2002.

[21] R. Manduchi, A. Castano, A. Talukder, and L. Matthies. Obstacle detection and terrain classification for autonomous off-road navigation. *Autonomous Robots*, 18:81–102, 2005.

[22] J. Lalonde, N. Vandapel, D. Huber, and M. Hebert. Natural terrain classification using three-dimensional ladar data for ground robot mobility. *Journal of Field Robotics*, 23(10):839 – 861, November 2006.

[23] R. Gonzalez and R. E. Woods. *Digital Image Processing*. Prentice Hall, 2002.

[24] R. Haralick and G. Shapiro. *Computer and Robot Vision*. Addison-Wesley, 1992.

[25] D. Anderson and G. McNeil. Artificial neural networks technology. http://www.dacs.dtic.mil/techs/neural/neural_ToC.php, August 1992.

[26] K. Z. Mao, K. C. Tan, and W. Ser. Probabilistic neural-network structure determination for pattern classification. *IEEE Transactions on Neural Networks*, 11(4):1009–1016, July 2000.

[27] R. O. Duda, P. E. Hart, and D. G. Stork. *Pattern Classification*. Wiley-Interscience, 2000.